Received: 21 March, 2023, Revised: 05 April 2023, Accepted: 06 April, 2023, Online: 28 April, 2023

DOI: https://doi.org/10.55708/js0204002

An Advanced Load-Line Analysis Software for use in the Design and Simulation of Microwave Low-Distortion, High-Efficiency and High-Power GaN HEMT Amplifiers

Yasushi Itoh*, **Takana Kaho**, **Koji Matsunaga**

Faculty of Engineering, Shonan Institute of Technology, Fujisawa 251-8511, Japan
*Corresponding author: Yasushi Itoh, 1-1-25 Tsujido-Nishikaigan, Fujisawa, Kanagawa, Japan, itoh@elec.shonan-it.ac.jp

ABSTRACT: An advanced load-line analysis software is devised for nonlinear circuit design and simulation of microwave low-distortion, high-efficiency and high-power GaN HEMT amplifiers. A single software package can incorporate DC, small- and large-signal performances of GaN HEMT devices, and then analyze nonlinear performance of amplitude-to-amplitude (AM-AM) and amplitude-to-phase (AM-PM) modulations, and finally evaluate intermodulation distortion (IMD) and error vector measurement (EVM). High speed and high accurate simulation become available with the use of behavioral modeling for representing nonlinear performance of GaN HEMT devices. In addition, the software employs a time-domain analysis using time-varying electrical waveform and thus give clear and deep insight into the nonlinear behavior of GaN HEMT devices as well as the nonlinear circuit design technique of low-distortion and high-efficiency amplifiers. In comparison with the harmonic-balance (HB) method, comparable performances have been successfully achieved for an L-band 10W GaN HEMT amplifier.

KEYWORDS: Load-Line Analysis, Low-Distortion, High-Efficiency, Power Amplifier, Microwave, Nonlinear Circuit Analysis, GaN HEMT

1. Introduction

In recent years, low-distortion and high-efficiency of microwave high-power amplifiers represent one of the most crucial design issues in order to meet the stringent requirements of reduced cost and excellent thermal treatment of the modern wireless transmitting systems. As a starting point of power amplifier (PA) designs, the Cripps load-line theory [1] is widely used to know available output power and efficiency as well as load conditions. The Cripps load-line theory, however, has adopted the simplified device description and thus strong nonlinearity including hard saturation, large leakage current and low-frequency dispersion effects of GaN HEMT devices cannot be accurately described [2-3]. Therefore, the PA designs utilize the active and/or passive load-pull measurements as a following step to know the optimum load impedances under the actual operating conditions [4]. The load-pull measurements are, however, limited by frequency, power, impedance range, number of harmonics and stability [5]. Therefore, most of the PA designs move to the nonlinear circuit simulations using harmonic-balance method [6]. The harmonic-balance method requires the accurate nonlinear device models. Indeed, the load-pull measurement and the harmonic-balance simulation are actually a powerful tool for PA designs but only a few information on the PA designs related to low-distortion and high-efficiency can be derived. On the other hand, the load-line theory is based on time-domain waveform analysis and thus provides much useful information on load and bias conditions for low-distortion and high-efficiency.

The author has presented the nonlinear load-line analysis method to demonstrate AM-AM and AM-PM characteristics of GaAs MESFET devices in 1995 [7] and in 2001 [8]. The method, however, cannot deal with strong nonlinearity such as hard saturation and large leakage currents. Moreover, the method is based on the measured data and thus time-consuming and inaccurate simulations were crucial design issues. In order to address these design issues, behavioral modeling is utilized to represent nonlinearity of GaN HEMT devices. Moreover, the calculated AM-AM and AM-PM characteristics are represented by behavioral modeling. It makes available the 2-tone power series and envelope analyses including IP and IMD as well as EVM [9] evaluation of the modern wireless transmitting systems with high speed and high accuracy. The load-line analysis method presented here can be performed to run software written by MATLAB R2021b [10]. This is the first nonlinear load-line analysis software package ever reported. An L-band 10W GaN HEMT amplifier has been designed by using this software and compared with the harmonic-balance method [6] to make sure the validity of the software.

2. Advanced Techniques in Load-Line Analysis

2.1. Time-Varying Electrical Waveform Analysis

Principles of the load-line analysis is shown in Figure 1 [7]. Drain current $I_d(t)$ and drain voltage $V_d(t)$ swing on the load-line having a resistive slope of -gl within the area surrounded by V_k (Knee voltage), V_{br} (breakdown voltage), $V_{br}+V_p$ (V_p is a pinchoff voltage) and zero. As a magnitude of $I_d(t)$, denoted as A(J), increases with input power, the upper or the lower-half of $I_d(t)$ is clipped by I_{dss} or zero. That is, DC component of $I_d(t)$ expanded by Fourier series increases or decreases. It means that the initial bias point ***a*** (V_{do}, I_{do}) moves to a different bias point. For example, under class-AB or B operation, the lower half of $I_d(t)$ is clipped first. DC component increases and the bias point moves upward in conjunction with the load-line. Next the upper-half of $I_d(t)$ is clipped. DC component decreases and the bias point moves downward in conjunction with the load-line. This procedure is repeated until the bias point converges to some quiescent bias point ***b*** (V_{do}, I_{dav}).

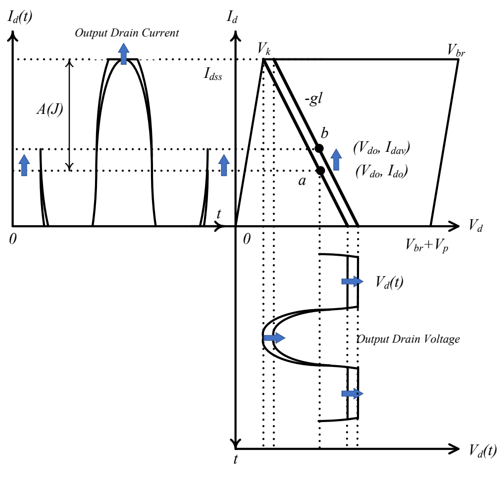

Figure 1: Principles of the load-line analysis. Drain current $I_d(t)$ and drain voltage $V_d(t)$ swing on the load-line having a resistive slope of -gl within the area surrounded by V_k (Knee voltage), V_{br} (breakdown voltage), $V_{br}+V_p$ (V_p is a pinchoff voltage) and zero. Point ***a*** is an initial bias condition (V_{do}, I_{do}). Point ***b*** is a final bias condition (V_{do}, I_{dav}).

$I_d(t)$, $V_d(t)$, a dynamic load-line are calculated by this load-line analysis software for GaN HEMT devices with V_k of 2V, V_{br} of 100V, V_p of -2V and I_{dss} of 2.14A, which is shown in Figure 2(a). As A(J) increases from 0.2 to 2.2A, $I_d(t)$ and $V_d(t)$ also increase and the bias point moves upward from the initial point (10V, 0.214A) in conjunction with the load-line. The slope of -gl can be varied as a dynamic load-line but keep constant in this case. Output power (P_{out}), drain efficiency (η_d), DC consumption power (P_{dc}) and V_d x I_d can be calculated for a variation of A(J) and plotted in Figure 2(b). As A(J) increases, P_{out} goes up to 10W and η_d also increases.

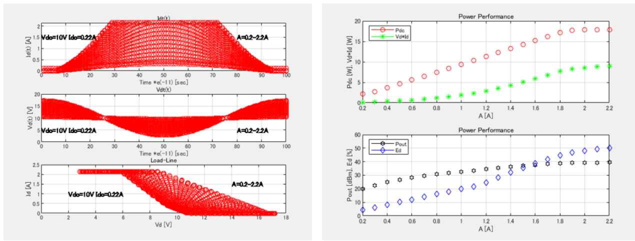

(a) (b)

Figure 2: (a) Calculated $I_d(t)$, $V_d(t)$ and dynamic load-line. (b) Calculated P_{out}, η_d, P_{dc} and V_d x I_d for GaN HEMT devices with V_k of 2V, V_{br} of 100V, V_p of -2V and I_{dss} of 2.14A

2.2. Large-Signal GaN HEMT Model Used in the Analysis

A large-signal GaN HEMT model is employed in the analysis, which is shown in Figure 3. Nonlinear circuit elements are transconductance (gm), drain-to-source resistance (R_{ds}), gate-to-source capacitance (C_{gs}) and gate-to-drain capacitance (C_{dg}), which are obtained from I-V curves as a function of the gate voltage (V_g) and the drain voltage (V_d). A forward gate current (I_{gs}) and a backward gate leakage current (I_{dg}) are also included in the analysis for hard saturation and large leakage conditions. The nonlinear circuit elements (gm, R_{ds}, C_{gs}, C_{dg}) and the gate current (I_{ds} and I_{dg}) are basically represented by behavioral modeling [11].

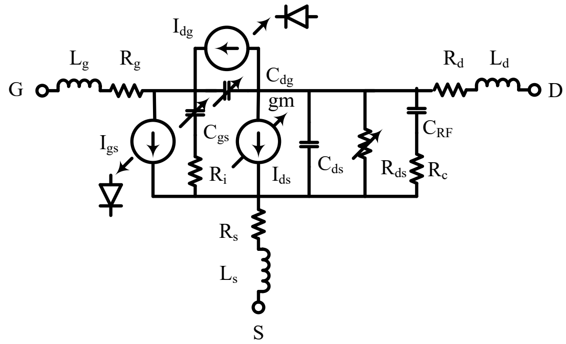

Figure 3: Large-signal GaN HEMT model. L_g, R_g, L_s, R_s, L_d and R_d are an extrinsic element, which are linear and thus keep a constant value. On the other hand, R_i, C_{ds}, C_{RF} and R_c are an intrinsic element, which are also linear and thus keep a fixed value. R_{ds} is used to represent DC characteristics. Therefore, RF characteristics are represented by $1/(1/R_{ds}+1/R_c)$ for a large value of C_{RF}.

Nonlinear circuit elements of gm, R_{ds}, C_{gs} and C_{dg} are obtained from I-V curves as a function of V_g and V_d, which is shown in Figure 4. Since $I_d(t)$ moves on the load-line with A(J), gm and g_{ds} (=1/R_{ds}) defined by (1) and (2) varies with A(J). Under large-signal operation, therefore, gm and gds are represented as an averaged value for one period, which are given as gm_{ave} and g_{dsave} by (3) and (4) [8]. I_d (V_g, V_d) is represented by behavioral modeling in place of the measured data for high speed and high accurate calculation. The Curtice Cubic Model [12] is used here.

$$gm = \lim_{\Delta V_g \to 0} \frac{I_d(V_g+\Delta V_g, I_d) - I_d(V_g, I_d)}{\Delta V_g} \quad (1)$$

$$g_{ds} = \lim_{\Delta V_d \to 0} \frac{I_d(V_g, V_d + \Delta V_d) - I_d(V_g, V_d)}{\Delta V_d} \quad (2)$$

$$gm_{av} = \frac{1}{T}\int_0^T gm(t)dt = \frac{1}{N}\sum_{n=1}^{N} gm(n) \quad (3)$$

$$g_{dsav} = \frac{1}{T}\int_0^T g_{ds}(t)dt = \frac{1}{N}\sum_{n=1}^{N} gds(n) \quad (4)$$

C_{gs} and C_{dg} defined by (5) and (6) also varies with A(J) on the load-line. Under large-signal operation, therefore, C_{gs} and C_{dg} are represented as an averaged value for one period, which are given as C_{gsave} and C_{dgave} by (7) and (8) [9-10]. In (5) and (6), C_{gs} and C_{ds} utilize the Statz model [13].

$$C_{gs} = C_{gs1} + \frac{C_{gs0}}{\left(1 - \frac{V_g}{V_{bi}}\right)^m} + C_{gs2}V_d \quad (5)$$

$$C_{dg} = C_{dg1} + \frac{C_{dg0}}{\left(1 - \frac{V_d - V_g}{V_{bi}}\right)^n} \quad (6)$$

$$C_{gsav} = \frac{1}{N}\sum_{l=1}^{N} C_{gs}(l) \quad (7)$$

$$C_{dgav} = \frac{1}{N}\sum_{l=1}^{N} C_{dg}(l) \quad (8)$$

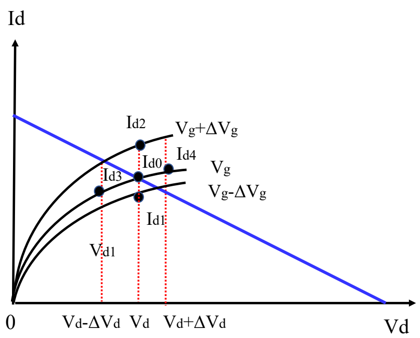

Figure 4: Nonlinear circuit elements of gm, R_{ds}, C_{gs} and C_{dg} obtained from I-V curves as a function of V_g and V_d

DC, small-signal, large-signal circuit elements as well as nonlinear capacitances consisting of Figure 3 can be read from Microsoft Excel sheet, which are shown in Tables 1(a), 1(b), 1(c) and 1(d), respectively. With the use of these data, gm_{ave}, g_{dsave} C_{gsave} and C_{dgave} are calculated and plotted in Figure 5. It is clearly shown that nonlinear elements are drastically change with A(J).

Table 1: DC, small-signal, large-signal circuit elements as well as nonlinear capacitances consisting of Figure 3

(a)

2mm_HEMT_R06.xlsx

	A	B
	mmHEMTR06	
	Vk	VarName2
	テキスト	数値
1	Vk	2
2	Vbr	100
3	Idss	2.1400
4	Vdo	10
5	Ido	0.2140
6	gl	0.2675
7	N	100

(b)

2mm_HEMT_R06.xlsx

	A	B
	mmHEMTR06S1	
	gm	VarName2
	テキスト	数値
1	gm	0.8963
2	cgs	1.7400e-12
3	cdg	3.0800e-13
4	cds	9.1200e-14
5	ri	0.1200
6	rds	40.8000
7	Rg	1.2300
8	Rs	1.2900
9	Rd	1.6000
10	Lg	5.0000e-12
11	Ls	3.0000e-11
12	Ld	4.0000e-12

(c)

2mm_HEMT_R06.xlsx

	A	B
	mmHEMTR06S2	
	A0c	VarName2
	テキスト	数値
1	A0c	1.2000
2	A1c	0.5200
3	A2c	-0.0136
4	A3c	-0.0178
5	ac	0.7000
6	bc	0.0100
7	Vdoc	10
8	Vboc	100
9	Vbic	0.6030
10	R1c	6500
11	R2c	0
12	RF	1.7850

(d)

2mm_HEMT_R06.xlsx

	A	B
	mmHEMTR06S3	
	vbi	VarName2
	テキスト	数値
1	vbi	0.6030
2	m	0.7000
3	cgs0	1.7520e-12
4	cgs1	0
5	cgs2	2.0000e-13
6	n	0.0100
7	cdg0	3.0800e-13
8	cdg1	0

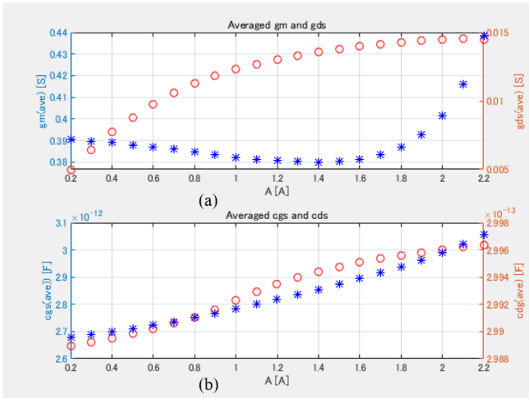

Figure 5: Calculated gm_{ave}, g_{dsave} C_{gsave} and C_{dgave}. Under class-B operation with a tuned load, $I_d(t)$ moves partly on the load-line with zero gm. Thus, the averaged gm sometimes decreases with A(J). However, the bias point moves upward and the averaged current also increases with A(J). Then gm drastically increases.

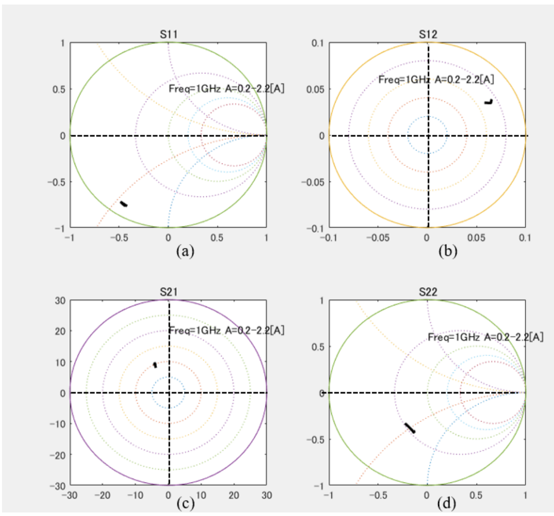

Figure 6: Large-signal S-parameters of GaN HEMT devices for A(J) from 0.2 to 2.2A at 1GHz.

Since gm_{ave}, g_{dsave}, C_{gsave} and C_{dgave} are obtained for each A(J), S-parameters of Figure 3 can be calculated, which is shown in Figure 6. A calculation was done for A(J) from 0.2 to 2.2A at 1GHz. Amid these parameters, S_{22} changes remarkably. A variation of Mag(S_{21}) and Ang(S_{21}) leads to AM-AM and AM-PM performances. In conjunction with the data in Figure 2(b), the output power (P_{out}), power gain (G_p), drain efficiency (η_d), power-added efficiency (η_{add}) and insertion phase variation ($\Delta\phi$) are calculated and plotted in Figure 7.

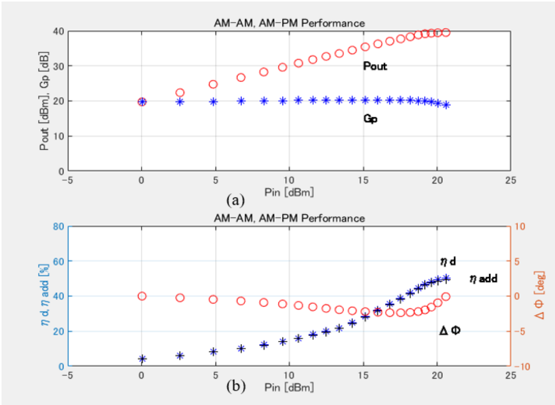

Figure 7: Calculated output power (P_{out}), power gain (G_p), drain efficiency (η_d), power-added efficiency (η_{add}) and insertion phase variation ($\Delta\phi$)

2.3. *Behavioral Modeling*

Once AM-AM and AM-PM performance are known, the distortion analyses including 2-tone power series analysis, 2-tone envelope analysis and EVM evaluation become available. Before the distortion analysis, AM-AM and AM-PM performances have to be represented by behavioral modeling for high speed and high accurate calculation. Behavioral modeling is listed in Table 2 [11]. The traditional distortion analysis of microwave power amplifiers deals with polynomial regression such as power series or Volterra series [1] because harmonic contents are easily handled. Thus, polynomial regression is employed here as behavioral modeling for representing AM-AM (P_{out} vs P_{in}) and AM-PM ($\Delta\phi$ vs P_{in}) performances shown in Figure 8.

Table 2: List of behavioral modeling: Behavioral modeling includes regression analysis and curve-fitting technique

Regression Analysis	Curve-Fitting Technique
Linear regression	Asymptotes slope
Logarithmic regression	Left hand technique
Power function regression	Right hand technique
Exponential regression	Build curve-fit function
Polynomial regression	Taylor's expansion
	Spline curve-fit technique

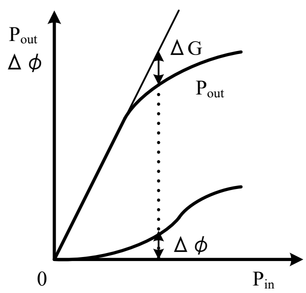

Figure 8: AM-AM and AM-PM performances of microwave power amplifiers. ΔG is a compressed gain and $\Delta\phi$ is an insertion phase variation, that is, a phase distortion

Based on the AM-AM (P_{out} vs P_{in}) and AM-PM ($\Delta\phi$ vs P_{in}) performances of Figure 7, the 3rd polynomial equations are calculated, which are shown in (9) and (10). P_{in} and P_{out} are denoted as antilog value. $\Delta\phi$ is given as degree.

$$P_{out} = a_3P_{in}^3 + a_2P_{in}^2 + a_1P_{in} + a_0 \tag{9}$$
$$a_3 = -5.8643E3$$
$$a_2 = 0.5233E3$$
$$a_1 = 0.0946E3$$
$$a_0 = 0$$

$$\Delta\emptyset = a_3P_{in}^3 + a_2P_{in}^2 + a_1P_{in} + a_0 \tag{10}$$
$$a_3 = -3.1400E3$$
$$a_2 = 1.2512E3$$
$$a_1 = -0.1019E3$$
$$a_0 = -0.0002$$

The calculated AM-AM and AM-PM performances shown in Figure 7 are also demonstrated in Figure 9 in conjunction with behavioral modeling. A good agreement has been achieved between the calculated and modeled data.

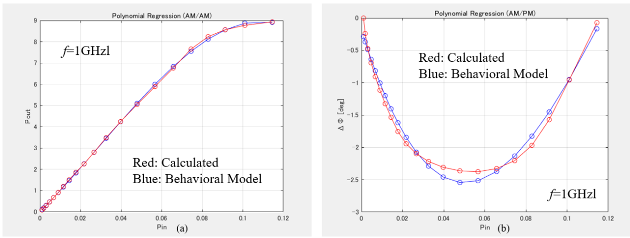

Figure 9: Calculated AM-AM and AM-PM performances combined with behavioral modeling. (a) AM-AM performance at 1GHz. (b) AM-PM performance at 1GHz. P_{out} and P_{in} are antilog number. $\Delta\phi$ is represented as degree

2.4. *Distortion Analysis (2-tone Analysis)*

This load-line analysis software prepares two types of 2-tone analyses: 2-tone power series analysis for weak nonlinearity and 2-tone envelope analysis for strong nonlinearity [1]. For example, in the 3rd-order 2-tone power series analysis, 2-tone signal described in (11) and (12) is inserted into (9). Then the 2nd-degree term of (9) produces the 2nd-order product at $2\omega_1$, $2\omega_2$, $\omega_1 \pm \omega_2$. The 3rd-degree term provides the 1st- and 3rd-order products at ω_1, ω_2, $3\omega_1$, $3\omega_2$, $2\omega_1-\omega_2$, $2\omega_2-\omega_1$. The 1st-, 2nd- and 3rd -order products are calculated and plotted as P_{in}-P_{out} in Figure 10. IIP_3 can be easily obtained from the intersection point of an extended linear part of ω_1 and an extended linear part of ω_3.

$$P_{in} = v_1 \cos\omega_1 t + v_2 \cos\omega_2 t \tag{11}$$

$$v_1 = v_2 = v \tag{12}$$

The 2-tone envelope analysis is shown in Figure 11 [1]. An envelope of the input 2-tone signal is modulated by a difference frequency of ω_1-ω_2 ($\omega_1 > \omega_2$). The amplified output signal is distorted in both magnitude and phase through AM-AM and AM-PM performances of PAs, which produces a serious intermodulation distortion. Input and output signals are given by (13) and (14). The input time-domain signal g(m) can be transformed from the frequency-domain signal G(k) by the inverse Fourier transformation as (15). The input signal is amplified and then the time-domain output signal g′(m) is given by (16). Finally, the frequency-domain output signal G′(k) is transformed by Fourier transformation as (17).

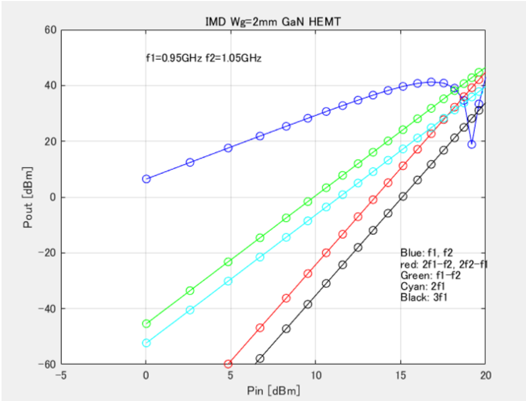

Figure 10: The 1st-, 2nd- and 3rd-order products. Red curve is the 3rd-order product ($2\omega_1$-ω_2 or $2\omega_2$-ω_1), which appear in close to carrier frequencies of ω_1 and ω_2.

$$V_i(t) = Re|\rho \cdot \exp(j\omega t)| \quad (13)$$

$$V_o(t) = Re|A(|\rho|) \cdot \exp(j\omega t + j\theta(|\rho|))| \quad (14)$$

$$g(m) = \sum_{k=0}^{N-1} G(k) exp\left(\frac{i2\pi mk}{N}\right) \quad (15)$$

$$g'(m) = |A(|g(m)|) \cdot \exp(j\theta(|g(m)|))| \quad (16)$$

$$G'(n) = \frac{1}{N}\sum_{k=0}^{N-1} g'(k) exp\left(-\frac{i2\pi nk}{N}\right) \quad (17)$$

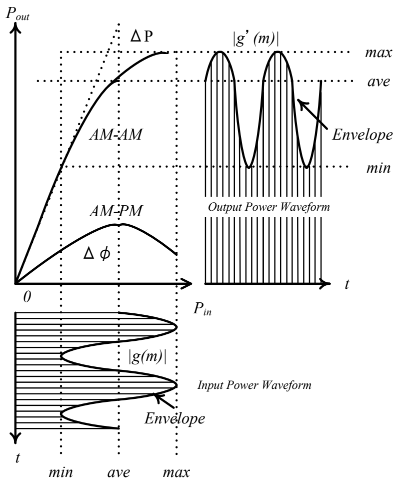

Figure 11: 2-tone envelope analysis. An envelope of input signal has a sinusoidal waveform beat by a difference frequency. An envelope of the amplified output signal is distorted in both amplitude and phase.

Time- and frequency-domain output signals are calculated with the use of 2-tone envelope analysis shown in Figure 11 and behavioral modeling of Figure 9 for 2-tone signal (f_1=0.9GHz, f_2=1.1GHz, v=0.02V) in (11) and (12), which are displayed in Figure 12. Figure 12(a) shows a time-domain output signal and Figure 12(b) displays a frequency-domain output signal (spectrum). IMD3 signals ($2f_1$- f_2 and $2f_2$- f_1) appear adjacent to carrier signals (f_1 and f_2). In addition, a difference signal (f_2- f_1), a sum signal (f_1+ f_2), 2nd-harmonic signals ($2f_1$ and $2f_2$) are also clearly shown. Due to the maximum limit of memory size of the computer, the resolution of spectrum becomes poor.

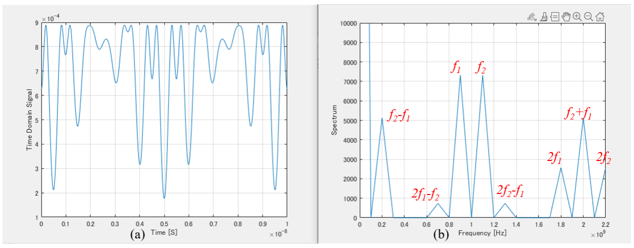

Figure 12: 2-tone envelope analysis: Time- and frequency-domain output signals are calculated for 2-tone signal (f_1=0.9GHz, f_2=1.1GHz, v=0.02V)

2.5. EVM Evaluation

Error vector magnitude (EVM) evaluation can provide a great deal of insight into the performances of digital communications transmitters and receivers [14]. The error vector is defined as a vector difference at a given time between the ideal reference signal and the measured signal, which is shown in Figure 13. AM-AM performance having ΔG and AM-PM performance having Δϕ in Figure 13(a) produce a serious vector error in Figure 13(b).

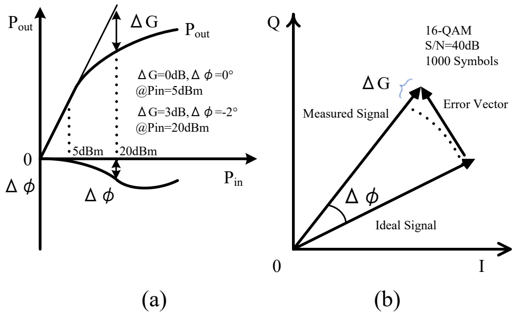

Figure 13: Error vector magnitude. (a) AM-AM and AM-PM data for use in the analysis. (b) Description on EVM schemes.

Now EVM is evaluated for GaN HEMT amplifiers having AM-AM and AM-PM performance shown in Figures 7, 9 and 13(a). EVM can be obtained by using MATLAB Simulink of EVM and MER measurement [15]. The explore model is used with an amplitude imbalance of 1 dB, a phase imbalance of 15 degrees and the DC offset of zero. Since the calculated AM-AM and AM-PM performances shown in Figures 7 and 9 cannot be used in the present form, the AM-AM and AM-PM data shown in Figure 9 are converted to a lookup table form. In the EVM analysis, 16-QAM modulated signal is used. S/N is assumed to be 40dB. EVM is evaluated at P_{in} of 5dBm for linear operation and 20dBm for nonlinear operation. Gain is 20dB at P_{in} of 5dBm and 17dB at P_{in} of 20dBm. The root-mean-square, maximum and peak values of EVM are listed in Table 3 and the constellation is demonstrated in

Figure 14. RMS value of EVM at P_{in} of 5dBm is much smaller than that of P_{in} of 20dBm, which means that a communication quality is higher because of low distortion conditions.

Table 3. Calculated root-mean-square (rmsEVM), maximum (maxEVM) and peak (pctEVM) values of EVM

Pin	5dBm	20dBm
rmsEVM[%]	2.9152	26.7234
maxEVM[%]	6.1943	40.2859
pctEVM[%]	22.8583	38.1610

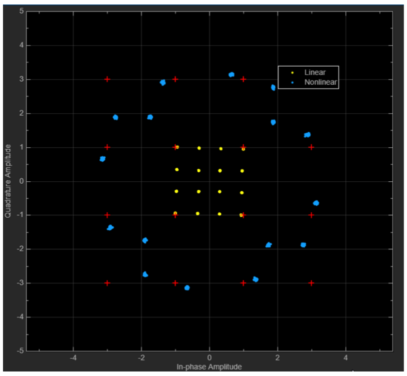

Figure 14: Constellation diagram of 16-QAM modulated signal. Red and blue dots are ideal and distorted signals at P_{in} of 20dBm. Red and yellow dots are ideal and distorted signals at P_{in} of 5dBm. It can be clearly shown that the constellation is seriously distorted at Pin of 20dBm (blue dots).

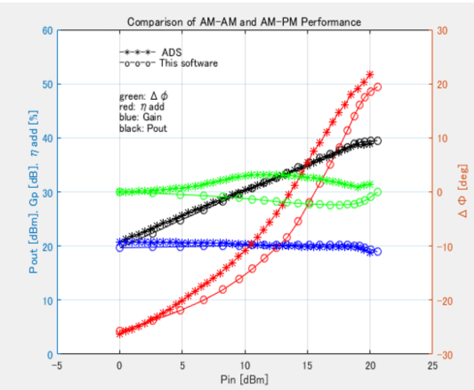

Figure 15: Comparison of the simulated power performances using the harmonic-balance simulator (ADS2021) and this load-line analysis software

3. Comparison with Harmonic Balance Method

An L-Band 10W GaN HEMT amplifier using Cree GaN HEMT CGH40010 [16] has been designed. Power performances are compared by using the harmonic-balance simulator (ADS2022 Keysight Technology) [17] and this load-line analysis software, which is shown in Figure 15. Output power and gain are in good agreement. Power-added efficiency and insertion phase variation are slightly different. These results demonstrate that the load-line analysis software introduced here is a candidate for the nonlinear analysis of GaN HEMT amplifiers. To verify the validity of the load-line software, the L-band 10W GaN HEMT amplifier is due to be actually fabricated and measured hereafter.

4. Comparative Analysis

A comparative analysis of the load-line method used in the microwave power amplifier is summarized in Table 4. A low-frequency I-V load-line measurement setup is shown in [2] and [3] to analyze low-frequency dispersion phenomena of GaN HEMT devices. The Cripps load-line theory is slightly modified to meet with low-voltage devices such as CMOS in [18] and [19]. That is, a slope of the load-line is adjusted for high efficiency in accordance with the knee voltage. By tilting a slope of the load-line for each cell of the distributed amplifier, high power and high efficiency over several octaves have been obtained [20] and [21]. The load-line is carefully chosen to achieve low-distortion and high-efficiency for both carrier and peaking amplifiers of the Doherty amplifier [22] and [23]. It must be noted that not only the load-line is carefully investigated but also time-varying waveform is checked in these load-line analyses. Similar to [2] and [3], a low-frequency I-V load-line is used to evaluate performance degradation of microwave transistor [24]. In addition, dynamic load-line is used in the design of narrowband and broadband amplifier designs [25] and [26]. This work presented here is based on a load-line analysis software, which can provide linear/nonlinear power and distortion performances. Therefore, this software can be considered to be useful to analyze various nonlinear power performance described in these References.

Table 4: Comparative analysis of the load-line method for use in the power amplifier design

Ref. No.	Year	Device	Load-line Method	Objective	Model
[2]	2009	800μm GaN HEMT	Low-frequency I-V load-line measurement	Analysis of low-frequency dispersion (i.e., traps and thermal effects)	Generic nonlinear equivalent-circuit model
[3]	2014	0.25 600 m GaN HEMT	Low-frequency I-V load-line measurement (2MHz)	Analysis of low-frequency dispersion	Behavioral Modeling of current generator
[18]	2018	GaN HEMT CGH160015D	Pedro load-line method	Impact of knee voltage effect and soft turn-on characteristic on the design of Class-B/J power amplifiers	Not described
[19]	2013	sub-micron CMOS	Extension of the load line theory to higher knee voltage value	Investigating the impact of the Knee-voltage on output-power and efficiency	Not described
[20]	2014	0.25 μm Al-GaN/GaN	Tilting load-lines	Design of uniform distributed power amplifiers having broadband high power	Not described
[21]	1987	200 μm GaAs FET	Emplying different load-line for each cell of distributed amplifier	Broadband high power distributed amplifier	Small--signal model
[22]	2008	Eudyna EGN010MK GaN HEMTs	Modulated load-line analysis	Analysis of saturated Doherty amplifier based on class-F amplifiers to maximize efficiency	OKI 0.1-W KGF1284 MESFET model
[23]	2008	Filtronic GaAs HEMT FPD750	Intrinsic load line of carrier and peak amplifier	WiMAX at 3.5 GHz is realized using a class AB amplifier	In-house Angelov non-linear model.
[24]	2021	Microwave Transistor	Low-frequency I-V and time-domain load-line measurement	Evaluation of microwave transistor degradation	Not described
[25]	2022	140nm GaN HEMT	Time-domain waveform analysis and dynamic load-line simulation	Accurate simulation of load-line and harmonic-balance methods	ASM-HEMT model
[26]	2023	GaN HEMT CGH40025F	Load-line analysis based on the series of continuum modes operation	Broadband amplifier design using class BJF-1	Not described
This Work	2023	Cree GaN HEMT CGH40010	Advanced load-line analysis for hard saturation large leakage current	Development of nonlinear load-line analysis software	Behavioral modeling

5. Conclusion

An advanced load-line analysis software for nonlinear circuit design and simulation of microwave low-distortion, high-efficiency and high-power GaN HEMT amplifiers has been presented. A single software package can incorporate DC, small-signal and large-signal performances of GaN HEMT devices, and then analyze nonlinear performance of AM-AM and AM-PM characteristics, and finally evaluate IMD and EVM. With the use of behavioral modeling, high speed and high accurate simulation become available. In addition, the software is based on a time-domain analysis using time-varying electrical waveform and thus can provide clear and deep insight into the nonlinear behavior of GaN HEMTs as well as the nonlinear circuit design of low-distortion and high-efficiency GaN HEMT amplifiers.

Acknowledgement

This research is based on a study commissioned by the National Institute of Information and Communications Technology, Japan ("Research and development on high-speed beam steering technology toward Beyond 5G" adopted number 06001).

References

[1] S. C. Cripps, *RF Power Amplifiers for Wireless Communication, 1st ED.*, Artech House, Norwood, MA, USA, 1999; pp. 24-32.

[2] A. Raffo, F. Scappaviva, G. A. Vannini, "New Approach to Microwave Power Amplifier Design Based on the Experimental Characterization of the Intrinsic Electron-Device Load Line", *IEEE Transaction on Microwave Theory and Techniques*, vol. 57, no. 7, July 2009

[3] A. Raffo, G. Bosi, V. Vadalà, G. Vannini, "Behavioral Modeling of GaN FETs: A Load-Line Approach", *IEEE Transaction on Microwave Theory and Techniques*, vol. 62, no. 1, January 2014

[4] Focus Microwaves Data Manual. Montreal, QC, Canada: Focus Microwave Inc., 1988.

[5] J. M. Cusak, S. M. Perlow, B. S. Perlman, "Automatic load contour mapping for microwave power transistors", *IEEE Trans. Microwave Theory Tech.*, vol. MTT-22, no. 12, pp. 1146–1152, December 1974.

[6] J. C. Rodringues, *Computer-aided Analysis of Nonlinear Microwave Circuits, 1st-ED.*, Artech House, Norwood, MA, USA, 1998; pp. 229-309.

[7] K. Mori, M. Nakayama, Y. Itoh, S. Murakami, Y. Nakajima, T. Takagi, Y. Mitsui, "Direct Efficiency and Power Calculation Method and Its Application to Low Voltage High Efficiency Power Amplifier", *IEICE Transaction*, vol. E78-C, no.9, pp.1229-1236, September 1995.

[8] Y. Ikeda, K. Mori, M. Nakayama, Y. Itoh, O. Ishida, T. Takagi, "An Efficient Large-Signal Modeling Method Using Load-Line Analysis and its Application to Non-Linear Characterization of FET", *IEICE Transaction*, vol. E84-C, no. 7, pp. 875-880, July 2000.

[9] Keysight Product Note 89400-14.

[10] MATLAB R2021B, Mathworks.

[11] T. R. Turlington, *Behavioral Modeling of Nonlinear RF and Microwave Devices, 1st ED.*, Artech House, Norwood, MA, USA, 2000, pp. 107-133.

[12] W. R. Curtice, M.A. Ettenberg, "Nonlinear GaAs FET Model for Use in the Design of Output Circuits for Power Amplifiers", *IEEE Transactions on Microwave Theory and Techniques*, vol. 33, no. 12, December 1985

[13] H. Statz, P. Newman, I. W. Smith, R. A. Pucel, A. Haus, "GaAs FET device and circuit simulation in SPICE", *IEEE Transactions on Electron Devices*, 1987, vol. 34, No. 2

[14] H. Jiang, P. Gong, W. Xie, B. Chen, B, H. Ma, C. Yang, "EVM Measurement and Correction for Digitally Modulated Signals", *2018 Conference on Precision Electromagnetic Measurements (CPEM 2018)*

[15] MATLAB Communication Toolbox, EVM Measurement.

[16] CGH40010, Wolfspeed, A Cree Company, USA

[17] Keysight Advanced Design System 2021

[18] X. Du, C. J. You, M. Helaoui, J. Cai, M. Ghannouchi, "Evaluation of Knee Voltage Effect and Soft Turn-on Characteristic on the Load Modulated Continuous Class-B/J Power Amplifier", *2018 IEEE MTT-S International Wireless Symposium (IWS)* 2018.

[19] P. Sandro, J. E. Mueller, R. Weigel, "Extension of the Load-Line Theory by Investigating the Impact of the Knee-Voltage on Output-Power and Efficiency", *Proceeding of the European Microwave Integrated Conferences*, pp. 488-491, 2013.

[20] M. Coers, W. Bosxh, "Analysis of Tilting Load-Line in AlGaN/GaN Broadband Uniform Distributed Amplifier", *Proceeding of GeMic*, 2014.

[21] M. L. Salib, D. E. Dawson, H. K. Hahn, "Load-Line Analysis in the Frequency Domain Distributed Amplifiers Design Examples", *IEEE MTT-S Digest*, pp. 575-578, 1987.

[22] J. Kim, J. Moon, Y. Y. Woo, S. Hong, I. Kim, J. Kim, B. Kim, "Analysis of a Fully Matched Saturated Doherty Amplifier with Excellent Efficiency", *IEEE Transaction on MTT*, vol 56, no. 2, pp. 328-338, February 2008.

[23] M. A. Medina, D. Schreurs, I. Angelov, B. Nauwelaers, "Doherty Amplifier Design for 3.5GHz Wimax Considering Load Line and Loop Stability", *Proceeding of the 3rd European Microwave Integrated Conference*, pp. 522-525, 2008.

[24] G. Bosi, V. Vadalá, R. Giofrè, A. Raffo, G. Vannini, "Evaluation of Microwave Transistor Degradation Using Low-Frequency Time-Domain Measurements", *2021 XXXIVth General Assembly and Scientific Symposium of the International Union of Radio Science (URSI GASS)*

[25] N. C. Miller, D. T. Davis, S. Khandelwal, F. Sischka, R. Gilbert, M. Elliott, R. C. Fitch, K. J. Liddy, A. J. Green, E. Werner, D. E. Walker, K. D. Chabak, "Accurate non-linear harmonic simulations at X-band using the ASM-HEMT model validated with NVNA measurements", *2022 IEEE Topical Conference on RF/Microwave Power Amplifiers for Radio and Wireless Applications (PAWR)*

[26] N. Poluri, M. M. D. Souza," Ease of Matching a Load Line Impedance in a 25 W Contiguous Mode Class BJF−1 Broadband Amplifier", *IEEE Microwave and Wireless Technology Letters*, 2023, Vol. 33, No.2.

YASUSHI ITOH received the B.S., M.S., and D.E. degrees in electronic engineering from Waseda University, Tokyo, Japan, in 1978, 1981, and 1989, respectively. He joined the Tokimec Inc. in 1981, where he has worked on the research and development of broadband low-noise amplifiers and oscillators. In 1990, he joined the Mitsubishi Electric Corporation, Information Technology R&D Center, where he has been engaged in the research and development of microwave and millimeter-wave low-noise and high power MMIC amplifiers and solid-state power amplifiers. In 2003, he joined the Shonan Institute of Technology, Kanagawa, Japan as a professor of the Faculty Engineering. From 2000 to 2003 along with 2020 to 2022, he has been a visiting professor of the University of Electro-Communications, Tokyo, Japan. From 2016 to 2018, he has been also a visiting professor of the National Chiao Tung University, Hsinchu, Taiwan. In 2000, he received the Electronics Society Award from

IEICE Japan. He is s Senior Life Member of the IEEE. He is currently a researcher of the Shonan Institute of Technology.

TAKANA KAHO is a Professor of Department of Electrical and Electronic Engineering, Shonan Institute of Technology. She received the B.S. and M.S. degrees in physics from Tokyo Metropolitan University, Japan, in 1994 and 1996 respectively. She received the Dr. Eng. degree in communication engineering from Tokyo Institute of Technology, Japan, in 2007. From 1996 to 2019, she was engaged in research on satellite equipment and MMICs at NTT Laboratories. Since 2009, she has been an Expert Committee Member on the Information and Communications Council of the Ministry of Internal Affairs and Communications, Japan. From 2010 to 2012, she was a Visiting Associate Professor at Research Institute of Electrical Communication, Tohoku University, Sendai, Japan. From 2014 to 2017, she has been a Visiting Associate Professor at Graduate School and Faculty of Information Science and Electrical Engineering, Kyushu University, Fukuoka, Japan. From 2016 to 2019, she was a Visiting Professor at Graduate School of Information Science and Technology, Osaka University, Osaka, Japan. Dr. Kaho is a senior member of the IEICE. She received the Japan Microwave Prize at the 1998 Asia Pacific Microwave Conference and the Young Researchers' Award in 2004 presented by IEICE. She received a Best Paper Award from IEICE in 2015, and 2017.

KOJI MATSUNAGA received the B.S. and M.S. degrees in physics from University of Tsukuba, Ibaraki, Japan, in 1987 and 1989, respectively, and the Dr. Eng. degree in electronics engineering from Kyoto University, Kyoto, Japan, in 2009. He joined NEC Corporation, Kanagawa, Japan, in 1989, where he was engaged in the research and development of III–V compound high frequency semiconductor devices. Since 1992, he has been engaged in the research and development of microwave and millimeter-wave high power amplifiers, wireless systems using GaAs or GaN III–V compound high frequency semiconductor devices. From 2013 to 2018, he also advanced research in power electronics. Since 2021, he has been with the Department of Electrical and Electronics Engineering, Shonan Institute of Technology, Kanagawa, Japan, where he is currently a professor. He received the Ohm Technology Award in 2011. His current research interests include microwave integrated circuit designs and wireless power transmission systems. Dr. Matsunaga is a member of the IEEE Microwave Theory and Techniques Society. He is also a senior member of the Institute of Electronics, Information and Communication Engineers, Japan.